The Journal of the Astronautical Sciences, Vol. 45, No. 4, October-December 1997, pp. 411–432

Minimum-Time Continuous-Thrust Orbit Transfers[1]

James D. Thorne[2] and Christopher D. Hall[3]

Abstract

To solve the minimum-time orbital transfer problem under continuous thrust, initial values of the Lagrange costates are required in the calculus of variations formulation. Assuming circle-to-circle transfer, expressions are developed for the approximate values of the optimal initial costates, which are then used as starting guesses for the associated two-point boundary value problem. The optimal initial costates are modeled as functions of the thrust and final radius in canonical units. These approximations work for noncircular destination orbits, as well as for noncoplanar transfers. Examples are provided for coplanar and noncoplanar orbital transfers. A dynamic step limiter is also presented which improves convergence in the shooting method.

Introduction

Optimal continuous-thrust problems have been investigated by many researchers, resulting in a broad range of publications which are too numerous to list in their entirety [1–5]. Two popular approaches to solving two-point boundary value problems (TPBVP) are direct and indirect methods. To guarantee mathematically that one has found the *optimal* solution to the TPBVP, it is necessary to propagate the adjoint variables or Lagrange costates according to their governing differential equations as provided by the calculus of variations. This is an example of an indirect method, which generally suffers from extreme sensitivity to the unknown initial values of the costates. Direct methods, on the other hand, do not require costates to find nonoptimal solutions. There are many important and very robust approaches based on direct methods [6, 7], but they do not give any

[1]This is a updated version of the paper presented at the AAS/AIAA Space Flight Mechanics Meeting, Austin, Texas, February 1996. This paper is declared a work of the U.S. Government and is not subject to copyright protection in the United States.

[2]Major, United States Air Force, Department of Aeronautics and Astronautics, Graduate School of Engineering, Air Force Institute of Technology/ENY, Wright-Patterson Air Force Base, OH 45433. Member AAS. Currently, Space and Missile Center/MTDG, Los Angeles Air Force Base, CA 90245.

[3]Assistant Professor of Aerospace and Systems Engineering, Department of Aeronautics and Astronautics, Graduate School of Engineering, Air Force Institute of Technology/ENY, Wright-Patterson Air Force Base, OH 45433. Senior Member AAS. Currently, Assistant Professor, Department of Aerospace and Ocean Engineering, Virginia Polytechic Institute and State University, Blacksburg, VA 24061.

guarantee of optimality because they do not use the adjoint variables to determine the control law. Direct methods may be used to find approximate values of initial costates through numerical perturbation from a known solution [8], but one must start with a reference trajectory that is close in some sense to the optimal solution. Thus, the classical choice left to the optimizer is to either use indirect methods with the possibility of nonconvergence due to extreme sensitivity to initial costate values, or to use direct methods and accept the possibility of finding a nonoptimal solution. However, if the initial values of the costates could be modeled approximately based on the problem parameters, one could overcome the sensitivity problems of indirect methods and obtain optimal solutions with confidence.

There are no models available in the literature that provide initial costate estimates for the minimum-time, continuous-thrust orbit transfer problem as explicit functions of the problem parameters. Others [11, 12] have tried, with limited success, to use the Hohmann transfer to initialize the Lagrange costates for the minimum-fuel problem with coasting arcs. However, the minimum-fuel problem allows for throttling and has a Lagrangian based on fuel mass, neither of which appear in the minimum-time problem. Thus, the minimum-fuel results provide no reliable information to initialize the costates in the minimum-time problem.

In this paper, we develop approximate models for the optimal initial costates and time of flight for minimum-time orbital transfers. For each orbital transfer, the thrust direction is allowed to vary, but the thrust magnitude is held at a constant maximum value as is indicated by choosing to minimize the flight time. The mass-flow rate is also assumed constant for any particular orbit transfer. However, we examine a wide range of thrust and mass-flow rate values by evaluating many numerical examples to form the approximate initial costate models. Assuming a circle-to-circle transfer, expressions are developed for the approximate values of the optimal initial costates. These approximations also work for noncircular end conditions as well as noncoplanar orbit transfers. The approximate initial costates are then used as starting values for the indirect approach. This way, the final result is a converged boundary value problem that produces the optimal control law.

The calculus of variations may be used to find the optimal control law for a spacecraft under continuous thrust. This development is not repeated here, but a good reference for it is the text by Bryson and Ho [10], which includes a numerical example of an Earth-to-Mars transfer under continuous thrust. The equations of the states, costates, and the optimal control law are repeated here. All quantities are expressed in canonical units [9], where the gravitational constant μ is unity regardless of the system under consideration as long as the initial circular radius is defined to be one distance unit (DU) and the initial circular velocity is one distance unit per time unit (DU/TU). The initial acceleration due to thrust is $A = a(t_0)$, and the final desired orbit radius is $R = r(t_f)$. In all examples, the initial spacecraft mass is one mass unit and the mass-flow rate is expressed in mass units per time unit. As shown in Fig. 1, the variable u is the time rate of change of the magnitude of the radius vector r, and v is the velocity component perpendicular to u. The thrust angle ϕ is measured from the spacecraft local horizon, which is in the direction of v. The variables λ_r, λ_u, and λ_v are the Lagrange multipliers, or costates, associated with the three state variables.

The Hamiltonian in these coordinates is:

$$\mathcal{H} = \lambda_r u + \lambda_u\left(\frac{v^2}{r} - \frac{\mu}{r^2} + a(t)\sin\phi\right) + \lambda_v\left(-\frac{uv}{r} + a(t)\cos\phi\right) \quad (1)$$

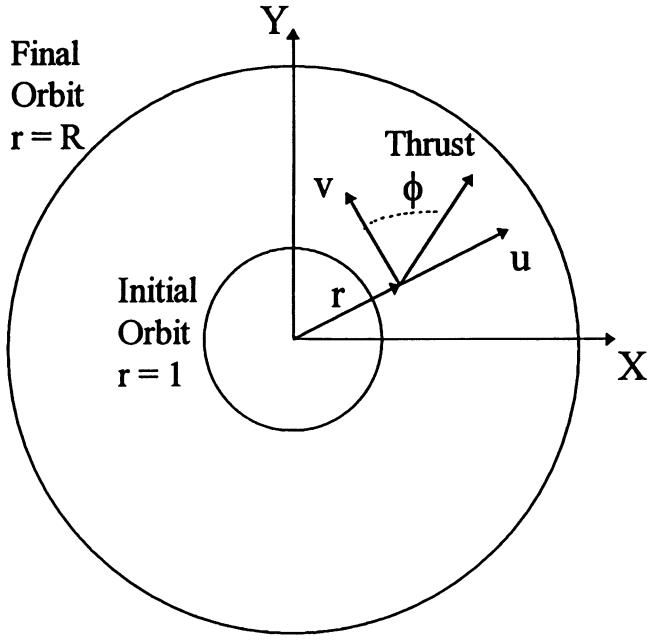

FIG. 1. Problem Geometry in Two Dimensions.

The differential equations for the states and costates are as follows [10]:

$$\dot{r} = u \tag{2}$$

$$\dot{u} = \frac{v^2}{r} - \frac{\mu}{r^2} + a(t)\sin\phi \tag{3}$$

$$\dot{v} = -\frac{uv}{r} + a(t)\cos\phi \tag{4}$$

$$\dot{\lambda}_r = -\lambda_u\left(-\frac{v^2}{r^2} + \frac{2\mu}{r^3}\right) - \lambda_v\frac{uv}{r^2} \tag{5}$$

$$\dot{\lambda}_u = -\lambda_r + \lambda_v\frac{v}{r} \tag{6}$$

$$\dot{\lambda}_v = -\lambda_u\frac{2v}{r} + \lambda_v\frac{u}{r} \tag{7}$$

where $a(t) = T/(m_0 + \dot{m}t)$. The optimal thrust angle ϕ is given by

$$\phi = \tan^{-1}\left(\frac{\lambda_u}{\lambda_v}\right) \tag{8}$$

Solutions to this set of equations are minimum-time arcs. Through the proper choice of initial costate values, the final state of the spacecraft may be matched to desired values. In all examples presented herein, $\lambda_r(0)$ is set equal to unity. Since the Hamiltonian is linear in the costates, an appropriate nonzero scaling factor may be used to make $\lambda_r(0) = 1$ without affecting the optimal control law.

Optimal Initial Costate Locus

In this section, the optimal initial Lagrange multipliers are modeled as functions of the problem parameters which include $R = r(t_f)$, the final radius, and $A = a(0)$, the initial thrust acceleration. This is accomplished by first examining the functional form of the costates graphically, then dividing the resulting locus into three distinct regions for separate analysis. Both analytical and empirical results are used to model the regions of the costate locus. The models are then evaluated by measuring the convergence sensitivity for the entire practical range of A and R.

The only way to find the optimal solution to the minimum-time boundary value problem is to guess some initial Lagrange costate values and hope for convergence. Even if one happens upon a convergent case to the desired final radius, it is unlikely that the parameter value of the thrust acceleration will match the spacecraft design. Then, the task is to adjust the value of A until it matches the desired value. If A is too large, it may be reduced by some small percentage, and used with the initial costate values from the known case. If the reduction percentage is small enough, the problem may converge for the new value of A. This process may be repeated until the desired value of A is achieved. The drawback to this continuation method [13] is that the step size for A to result in convergence is not constant, and one must therefore "hand-hold" the process by monitoring the convergence behavior through perhaps hundreds of small changes in A. Depending on the available computing power and sensitivity of the problem, this process could take days or weeks to complete. Furthermore, one must also have found a "seed" case to begin the search.

Suppose $R = 2$, and we have a converged case for $A = 100$. If A is multiplied by 0.9, then convergence may be achieved using the last values of the initial costates as the new starting guess. If this procedure is repeated for more than roughly 20 times, the shooting method will continue to take more iterations to converge, and eventually will not converge at all. Then, the multiplication factor must be increased to perhaps 0.95, and higher still as A decreases. This phenomenon is due to the sensitivity of the system to initial conditions, which increases for the increased flight times associated with small thrust values at a given R.

After solving a series of examples for large range of A, it is instructive to plot a locus of the converged initial values of the costates, one versus another, to examine their behavior. This is an original presentation technique [5, 14] which is shown in Fig. 2. This choice of axes is motivated by the polar thrust angle ϕ as shown in Fig. 1. The initial value of ϕ may be measured from the $\lambda_v(0)$ axis to a point on the locus with the vertex at the origin. Thus, the initial thrust angle may be seen relative to the spacecraft local horizon directly from the figure. For large values of A, the initial thrust angle $\phi(0)$ approaches 90 degrees, and for small values of A, $\phi(0)$ approaches zero degrees, in the spacecraft horizontal direction.

The process used to create the solid locus in Fig. 2 is repeated for different values of the mass-flow rate, and shown in Fig. 3. When $\dot{m} = -0.1$, the final time cannot exceed 10 time units, because all of the spacecraft mass would be consumed. Similarly, the final time cannot exceed 100 time units for $\dot{m} = -0.01$. Thus, the locus spiral terminates for some minimum value of A, because small values of A correspond to long flight times. When $\dot{m}$ is taken to be zero, there is no time limit for the powered trajectory, and any value of A may be used. Therefore, the $\dot{m} = 0$ locus continues spiraling indefinitely as A is reduced. It is

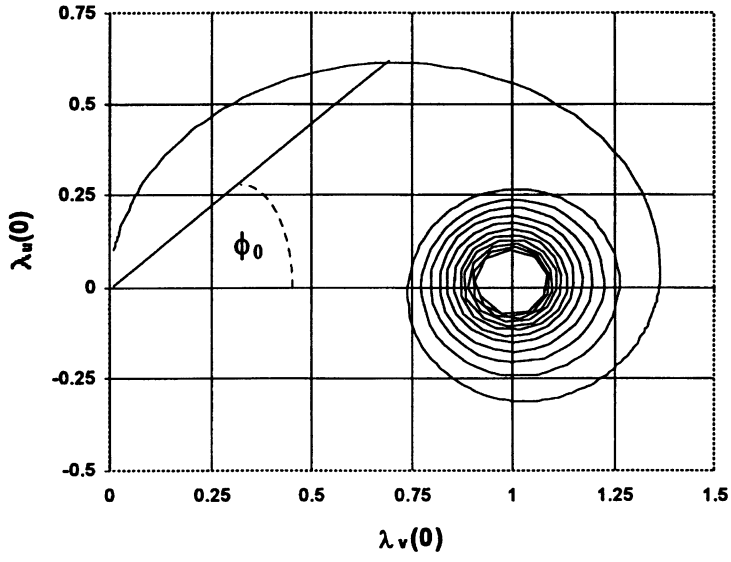

FIG. 2. Optimal Initial Costate Locus for $R = 2$, $\dot{m} = 0$.

clear from Fig. 3 that the changes in $\dot{m}$ have little effect on the location of the initial costates. A possible physical interpretation of this relative insensitivity to $\dot{m}$ is that mass-flow rate has no immediate effect at the initial time, since the spacecraft mass is normalized to unity at $t = 0$. Also, only small changes in the costates at the initial time are required for significant changes in the trajectory at the final time, due to the sensitivity of the problem. Based on observations from the numerically generated initial costate loci, the quantity $\dot{m}$ is not included in the costate models, in order to simplify the analysis.

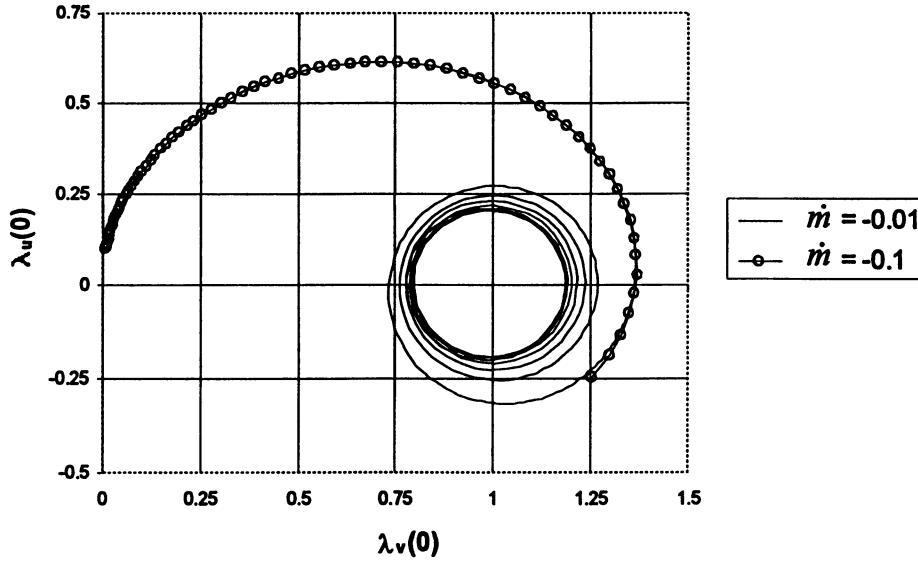

FIG. 3. Optimal Initial Costate Locus for $R = 2$, $\dot{m} = -0.01, -0.1$.

The next step is to take the numerical results of many converged cases with R and A as parameters, and plot the optimal initial costates as functions of R and A, forming the loci shown in Fig. 4. In this way, the functional behavior of the costates is easily seen to be represented by three distinct regions, which may be parameterized by the parameter S [15]:

$$S = \sqrt{(R - 1)/A} \tag{9}$$

The three regions correspond approximately to $S < 1$, $1 < S < 10$, and $10 < S$, as discussed below. The parameter S has the units of time, and is equal to one-half of the flight time on a rectilinear path between two stationary points in field-free space, given a thrust reversal at the exact midpoint of the trajectory.

Near the origin of the $\lambda_v(0)$, $\lambda_u(0)$ plane, the optimal initial costates lie on a nearly parabolic arc. As A decreases or R increases, S increases, and the locus moves away from the origin on this parabolic arc. With further increases in S, the locus becomes a nearly elliptical arc which transitions to a spiral centered at $\lambda_v = 1$, $\lambda_u = 0$. This point represents the limiting case of purely tangential thrust [2]. The optimal initial costate loci show a common tendency to spiral towards the point $(1, 0)$ with $\dot{m} = 0$. Two example points are shown in Fig. 4, which correspond to an asteroid intercept mission and the well-known Earth-to-Mars transfer example given by Bryson and Ho [10]. The parabolic, elliptic, and spiral regions of the costate locus are addressed separately for modeling purposes.

The parabolic region represents orbital transfers that take less than about one-quarter revolution to complete, either due to high thrust or small radius change. As developed in Thorne and Hall [5], the analytical approximations for the parabolic region of the costate locus are given by:

$$\lambda_u(0) \approx S \tag{10}$$

$$\lambda_v(0) \approx S^2 \tag{11}$$

$$t_f \approx 2S \tag{12}$$

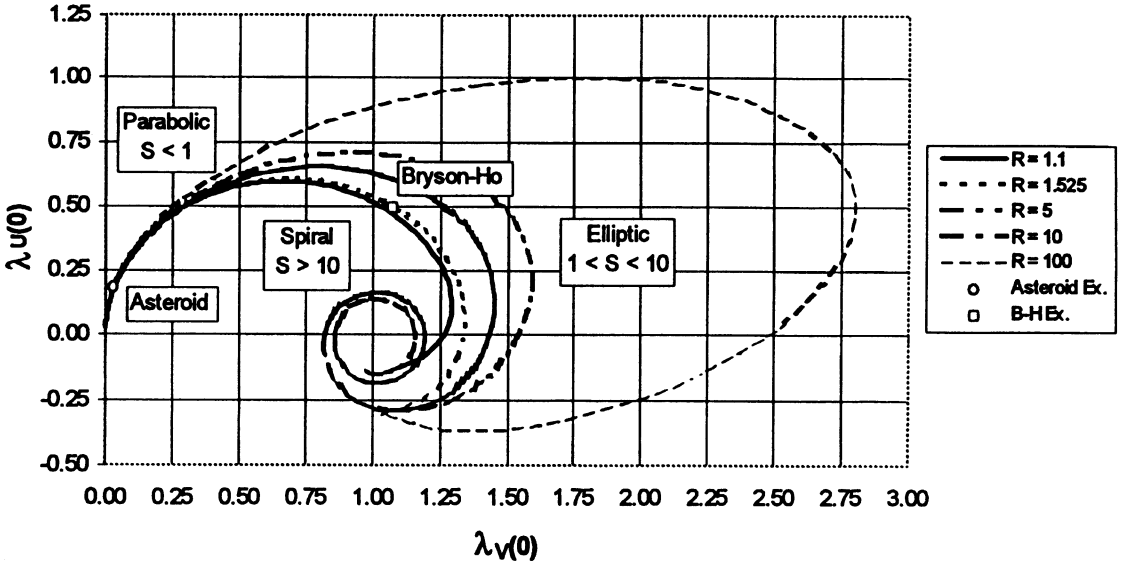

FIG. 4. Optimal Initial Costate Loci for R from 1.1 to 100.

It has been found from numerical studies that the parameter S must be equal to one or less in canonical units for the approximations in equations (10–12) to provide a reasonable first guess. The physical implication of the limit $S \leq 1$ is that the orbital transfer will occur in less than roughly one-quarter revolution.

If the transfer occurs in the neighborhood of one revolution, the initial costates do not lie near the parabolic arc or the point $(1, 0)$. In this case, the locus has a nearly elliptical shape as seen in Fig. 4, and the range of S is roughly $1 < S < 10$. The well-known Earth-Mars transfer example given in Bryson and Ho [10] lies in this region. In this case, the analytical approach taken in Thorne and Hall [5] is not applicable, although the expression for t_f given by equation (12) may still be used, because the time of flight exhibits less sensitive behavior in the transition region where $1 < S < 10$. Since there are only two parameters (A and R), we can numerically determine a parameterized curve fit for $\lambda_u(0)$ and $\lambda_v(0)$ in this region by assuming the polar description of an ellipse. Fitting the data to produce models for the eccentricity, semi-latus rectum, and true anomaly of the locus ellipses leads to the following approximate analytical expressions for $\lambda_u(0)$ and $\lambda_v(0)$:

$$\lambda_u(0) = r_{\text{ell}} \sin \theta_{\text{ell}} + 0.03588 \tag{13}$$

$$\lambda_v(0) = 0.165989 - r_{\text{ell}} \cos \theta_{\text{ell}} \tag{14}$$

where

$$\theta_{\text{ell}} = \frac{1.0}{(0.498719 - 0.811477R^{0.25})} A^{0.25} + \frac{1.0}{(0.279574 - 0.050554R^{-0.25})} \tag{15}$$

$$r_{\text{ell}} = \frac{-0.00091R + 0.4114}{1.0 + (0.00264R + 0.616)\cos(\theta_{\text{ell}} + 0.0008124R + 0.11876)} \tag{16}$$

This fit was obtained using approximately 1000 solutions for $1.1 < R < 100$, and $0.1 < S < 100$. An example of the parametric fit is shown in Fig. 5 for $R = 1.525$ and $R = 100$.

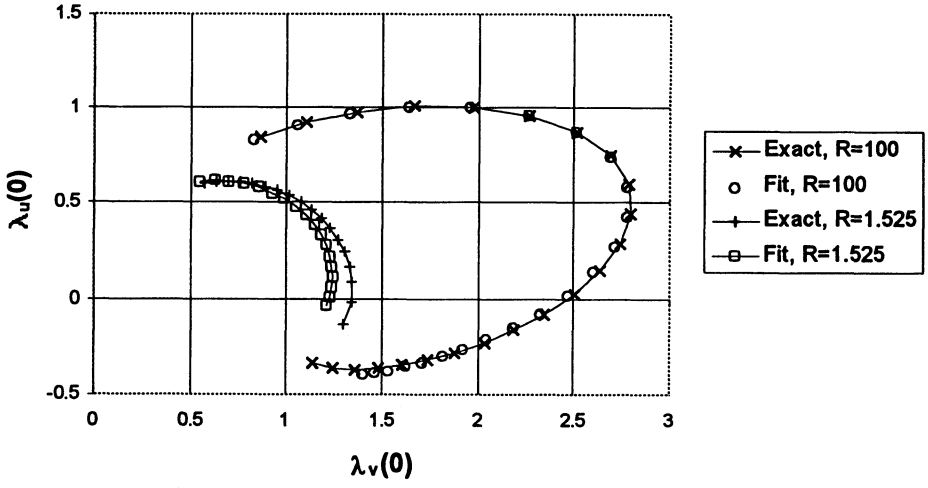

FIG. 5. Elliptic Fit for $R = 1.525$, 100.

The spiral region of the costate locus corresponds to problems with more than 10 revolutions, and it is well known [2] that the optimal thrust direction is nearly tangential to the path through most of the transfer. For such cases, a good starting guess is $\lambda_u(0) = 0$, and $\lambda_v(0) = 1$. This corresponds to an initial tangential thrust with $\phi = 0$, as seen in Fig. 4. The time of flight for a many-revolution transfer is approximately given by [2]:

$$t_f = \frac{1}{A}\left(1 - \frac{1}{\sqrt{R}}\right) \tag{17}$$

Solution of Boundary Value Problem

To solve the boundary value problem using the previous results, the parameter S is first calculated from equation (9). If $S \leq 1$, then equations (10–12) are used to initialize the problem. If $1 < S < 12$, then equations (12–14) provide a reasonable set of initial values for the problem. The parameter value of $S = 12$ is used to extend the elliptic costate model further into the spiral region. If $S > 12$, the initial values of the costates are close to $\lambda_u(0) = 0$ and $\lambda_v(0) = 1$. The approximate time of flight for this case is given by equation (17).

To improve the convergence properties for these problems, a simple modification is made to Newton's method by providing a variable scaling factor for the Newton step. If $\mathbf{P}$ is a vector of unknowns such as $\mathbf{P} = (\lambda_u(0), \lambda_v(0), t_f)$, and $\Delta\mathbf{P}$ is the Newton step, then the following equation is used:

$$\mathbf{P}_{i+1} = \mathbf{P}_i + \frac{\Delta\mathbf{P}_i}{1 + \|\Delta\mathbf{P}_i\|} \tag{18}$$

This modification provides a dynamic scaling effect on the Newton step. If $\|\Delta\mathbf{P}_i\|$ is large, the scaling limits the individual component changes to less than unity, without changing the step direction. If $\|\Delta\mathbf{P}_i\|$ is small, the scaling does not affect the magnitudes of the individual component changes very much, so the quadratic convergence rate is nearly maintained in the neighborhood of the solution point. The scaling preserves the direction of the Newton step in the search space, but prevents the magnitude from becoming unreasonably large, as can happen with nonlinear problems.

When used with the approximations for each region of the costate locus, the dynamic scaling leads to convergence using the shooting method [16] for the indicated ranges of R and A, and reasonable values of $\dot{m}$. Even with this rather simple search technique, satisfactory results are achieved by virtue of the accuracy of the approximate initial costate models.

Although the examples in this paper assume orbit raising, it is possible to accomplish orbit lowering by reversing and scaling the boundary conditions so that the lower orbit has a unit radius. The final costates at the lower orbit take the role of the initial costates, and may be approximated by the models given in this paper. The equations of motion are then propagated backwards in time using a negative time step from the lower to the higher orbit. Additionally, the final mass of the spacecraft must be calculated using the value of the flight time. Since an estimate of the final flight time is available for each iteration in the modified Newton step as described above, the final mass of the spacecraft can also be calculated for each iteration. During the backwards propagation, the mass of the spacecraft is increased for every negative time step, since the mass-flow rate is also negative.

Convergence Sensitivity

To measure the convergence sensitivity of the shooting method for various values of S and R, a plot of modified Newton method iterations is presented in Fig. 6. The number of iterations for a given R and A is a good measure of the success of the approximate models, since closer initial values require fewer iterations for convergence to a desired error tolerance. Generally, the sensitivity of the system increases with decreasing A and thus increasing S, because the flight times become much longer for a given R value. In other words, the "shots" become much longer in the shooting method. The initial values of the Lagrange costates tend to stay within the neighborhood of unity, as seen in Fig. 4. However, the flight time may become large for small A, so errors in the time models tend to be magnified for large values of S corresponding to multiple revolution transfers. This explains the increased system sensitivity for large S, but the modified Newton method will still converge using the models for the time and initial costates over the specified ranges of A and R. In Fig. 6, the S parameter is plotted on the horizontal axis using a logarithmic scale, and the three decades shown correspond to the three regions of the costate loci in Fig. 4. There are peaks in the sensitivity near $S = 1$ and $S = 12$, which occur in the transition regions between the parabolic, elliptic, and spiral point models for the approximate initial costates. Some of the curves do not span the entire range of S, because of the relationship $R = S^2A + 1$. For instance, on the curve of constant $A = 0.5$, $R = 201$ when $S = 20$. Since this value of R is larger than the range of the models, the data is stopped when R reaches a value of 100. The value of $R = 100$ is used as an upper limit because of physical considerations. In an Earth-centered system, the lunar orbit is at roughly 60 DU, based on the radius of the Earth. In a sun-centered system, the planet Pluto is at roughly 40 DU, based on the radius of the Earth's orbit about the sun. Thus, $R = 100$ DU is more than adequate to cover the range of currently practical missions.

It is important to recognize that the iteration numbers shown in Fig. 6 are based on the *approximate* costate models. If the boundary value problems represented

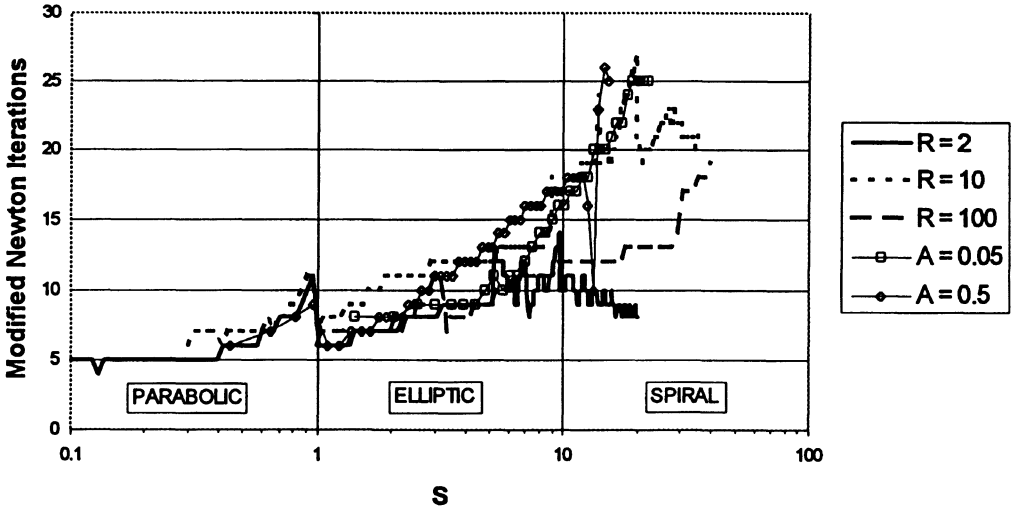

FIG. 6. Convergence Sensitivity to Initial Costate Model.

by each point on the curves had been solved by slowly varying the thrust as described at the beginning of this chapter, the step size could be kept small enough such that each case could be done in about five iterations. However, that technique requires a slow approach from some elusive known case to the case of interest. Using the approximate costate models provided here along with the modified Newton method, any case of interest may be solved directly with *no prior knowledge*. Thus, one may proceed immediately with any values of R and A to Fig. 6 and obtain a rough idea of how many iterations to expect using the modified Newton method and the approximate initial costate models. Without the initial costate approximations, it would be unreasonable to expect convergence *at all* for arbitrary values of R and A.

The extreme sensitivity of the minimum-time continuous thrust problem to the initial costate values is well documented [10]. As mentioned earlier regarding the continuation method [13], the step size in the problem parameter A must be constantly decreased to maintain convergence in a fixed number of iterations as the locus moves toward the center of the spiral region, where A approaches zero. This decreasing step size phenomenon is a direct measurement of the convergence sensitivity, but this also depends on the robustness of the search technique. Because of the interdependence of the model accuracy and the capabilities of search method, both the model and the modified Newton method are used to produce the iteration data shown in Fig. 6 instead of the continuation method. Clearly, a different initial costate model and search method will produce different iteration data. Thus, the convergence sensitivity shown in Fig. 6 is only intended to represent the behavior of the models and techniques presented here.

Two-Dimensional Examples

Asteroid Intercept Example

The first example involves a spacecraft design that has been investigated by past researchers [10]. A spacecraft is in orbit about the sun at $r(0) = 1$ AU, with a thrust of 0.1405 and a mass-flow rate of -0.07488, all in canonical units. Suppose it is desired to intercept an Earth-crossing asteroid at a distance of 500,000 miles outside the Earth's orbit. If the spacecraft is put into a circular orbit at $R = 1.005$, the velocity must be different than that of the Earth-crossing object when they meet, since there is no point where the velocity components will match each other. In this case, the quantity $S = \sqrt{(R - 1)/A} = 0.1866$, which is less than unity. Thus, the optimal initial costates should lie near the parabolic region of the costate locus, and the approximate initial values are given by equations (10) and (11). The approximate time of flight is given by equation (12). Using the above problem parameters, the results in canonical units are given in Table 1.

The first line in Table 1 is the set of initial approximations for the asteroid example. The first iteration is considered to be the evaluation of the approximate

TABLE 1. Asteroid Example

Iteration	t_f	$\lambda_u(0)$	$\lambda_v(0)$
1	0.377291	0.188646	0.035587
3	0.373630	0.184044	0.033189

models for the initial costates and time of flight. The second line shows the final, converged values after three iterations of the shooting method. The total thrusting time is roughly 21.5 days in physical units. In this case, the initial approximations for the costates and flight time are very close to the converged values, allowing for quick convergence. Figure 7 shows the iterative search history for the flight time and initial costates from the initial guess to the converged values.

Figure 8 compares the exact control angle history from the converged case with the approximate history generated by the initial estimates. Both curves pass through the zero angle, showing the switch in thrust direction. The differences between the initial estimates and the converged values are most evident here, since the costate histories are very sensitive to the initial conditions.

Figure 9 shows a comparison of flight path trajectories using the control law from the initial estimates and the converged values. In this case, the paths are almost identical in spite of the differences in the control angle histories. Thus, approximate initial costates obtained using the assumptions in Thorne and Hall [5] are sufficient to achieve an almost optimal trajectory.

Bryson and Ho Example

The second example is the well-known Earth-to-Mars orbital transfer case given in Bryson and Ho [10], where $R = 1.525$, $A = 0.1405$, and $\dot{m} = -0.07488$ mass units per TU. The initial costate values are not given in the reference. In this case, the quantity $S = 1.933$, so $1 < S < 10$. Thus, the optimal initial costates should lie in the elliptic region of the costate locus, and the approximate initial values are given by equations (13) and (14). The approximate time of flight is given by equation (12). Using these problem parameters, the results are shown in canonical units in Table 2.

The first line in Table 2 is the set of initial approximations for the Bryson and Ho example. The second line shows the final, converged values after seven iterations of the shooting method. The converged initial costate values are plotted in Fig. 4 as a point on the costate locus which is identified with the label "Bryson-Ho." The initial approximations for the costates and time of flight are still close

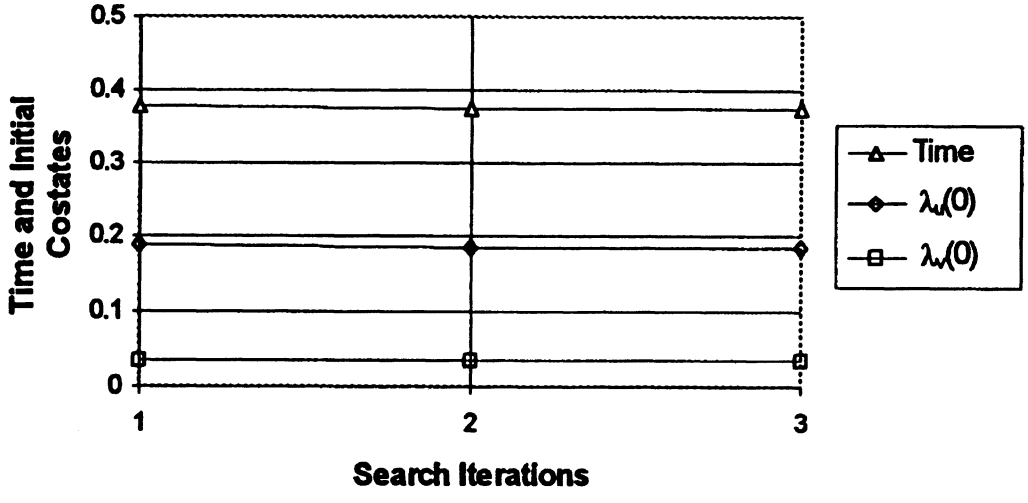

FIG. 7. Iterative Search History for Asteroid Example.

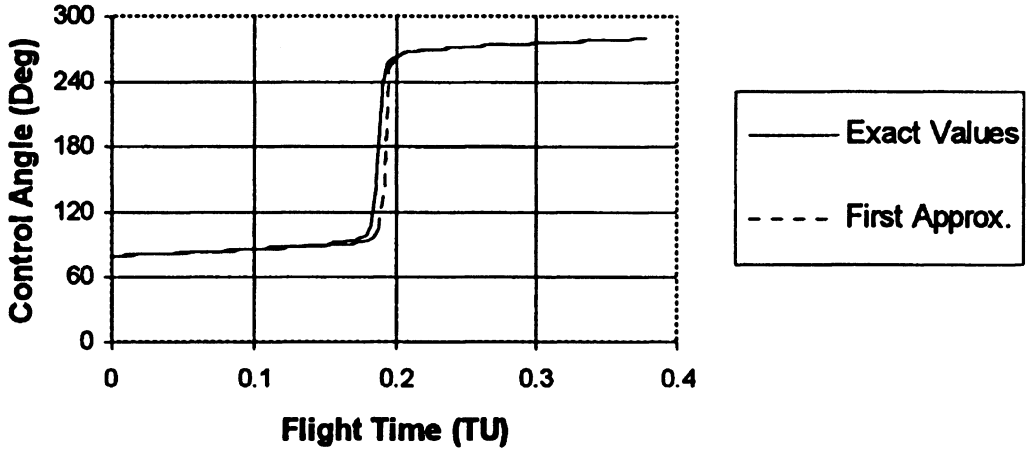

FIG. 8. Control Angle History for Asteroid Example.

to the converged values, but this example takes more iterations for convergence than the asteroid example. This is because the convergence sensitivity is greater in the elliptic region than in the parabolic region, and the initial approximations are not as close as in the asteroid example. However, the initial approximations are all within roughly 15% of the converged values, which is certainly better than no information at all.

Figure 10 shows the iterative search history for the flight time and initial costates in the Bryson and Ho example from the initial guess to the converged values. Figure 11 compares the exact control angle history from the converged case with the approximate history generated by the first and third iterations of the initial estimates. All curves pass through 180 degrees, showing the switch in thrust direction. As the search progresses, the control angle history approaches the optimal control angle solution. Again, the differences between the initial estimates and the converged values are most evident here, since the costate histories are very sensitive to the initial conditions.

Figure 12 shows three trajectories corresponding to the first, third, and seventh iterations in the shooting method to solve the Bryson and Ho example. The seventh iteration is considered the exact solution for this example. The trajectory from the

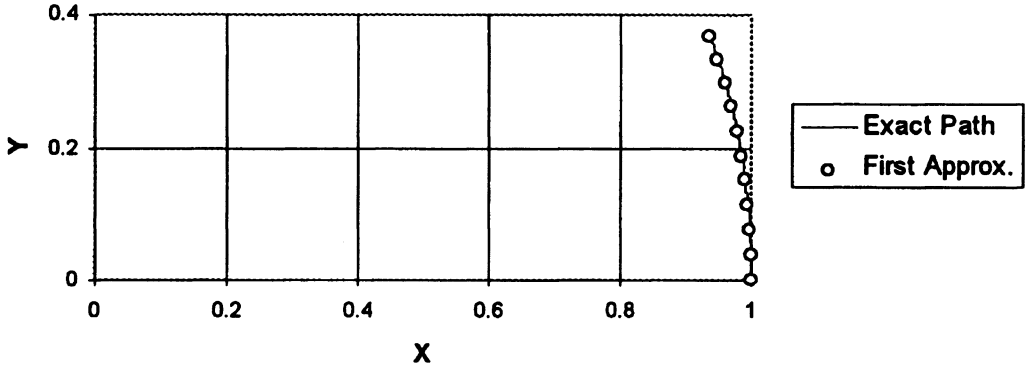

FIG. 9. Optimal Trajectory for Asteroid Example.

TABLE 2. Bryson and Ho Example

Iteration	t_f	$\lambda_u(0)$	$\lambda_v(0)$
1	3.8660858	0.4221273	1.1093899
7	3.3192600	0.4949228	1.0785465

first iteration overshoots the desired final radius by roughly 0.5 DU, and the third is much closer. The "in-track" error along the spacecraft velocity direction is dominant, and is sensitive to changes in the final flight time. This example shows typical behavior in which the final flight time is directly related to the final radius, assuming the errors are small. By this, we mean that a small increase in final time over that of the minimizing path will result in a small increase in R. Conversely, a small decrease from the optimal flight time will result in a small decrease in R.

The final radius value in the Bryson and Ho example is 0.52 AU larger than the one in the asteroid intercept example, but all remaining parameters are the same. These values are chosen to illustrate that a relatively small change in a single problem parameter may force one to use a different model for the approximate initial costates. This effect may be seen in Fig. 4 by comparing the locations of the labels "Asteroid" and "Bryson-Ho" on the locus curves.

Application to Three-Dimensional Problems

We now illustrate how to apply the foregoing results to three-dimensional problems. The equations of motion are most easily expressed using the right-handed cartesian system of x, y, and z coordinates, as shown in Fig. 13. The initial circular orbit lies in the x-y plane, and the initial position is at $x = 1$, $y = 0$, $z = 0$. The thrust direction must be defined with (at least) two angles. The angle α lies in the x-y plane, and is measured from the x-axis in the positive direction. The angle β is measured "up" from the x-y plane, and lies in the plane containing the thrust vector and the z-axis. The magnitude of the position vector

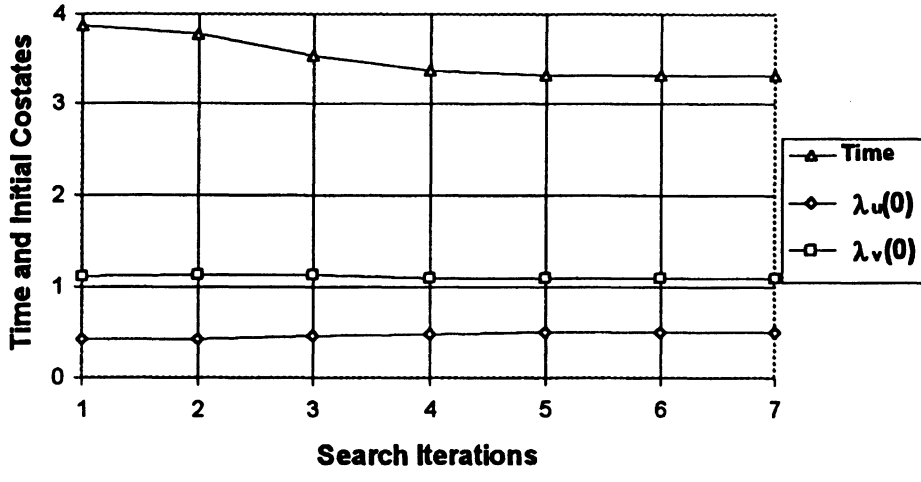

FIG. 10. Iterative Search History for Bryson and Ho Example.

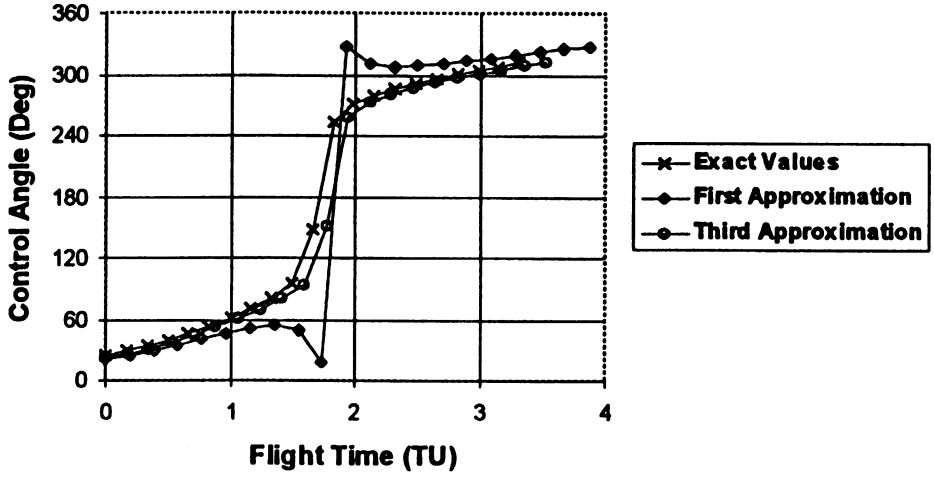

FIG. 11. Control Angle History for Bryson and Ho Example.

is r, and the thrust acceleration is A as defined previously. Using these definitions, the equations of motion are:

$$\ddot{x} = -(\mu/r^3)x + A\cos\beta\cos\alpha \tag{19}$$

$$\ddot{y} = -(\mu/r^3)y + A\cos\beta\sin\alpha \tag{20}$$

$$\ddot{z} = -(\mu/r^3)z + A\sin\beta \tag{21}$$

This leads to the following variational Hamiltonian:

$$\begin{aligned}\mathcal{H} =& \lambda_x\dot{x} + \lambda_y\dot{y} + \lambda_z\dot{z} + \lambda_{\dot{x}}[-(\mu/r^3)x + A\cos\beta\cos\alpha] \\ &+ \lambda_{\dot{y}}[-(\mu/r^3)x + A\cos\beta\sin\alpha] + \lambda_{\dot{z}}[-(\mu/r^3)x + A\sin\beta]\end{aligned} \tag{22}$$

The optimality condition [10] leads to two control laws for the thrust vector angles α and β:

$$\tan\alpha = \lambda_{\dot{y}}/\lambda_{\dot{x}} \tag{23}$$

$$\tan\beta = \lambda_{\dot{z}}/(\lambda_{\dot{x}}\cos\alpha + \lambda_{\dot{y}}\sin\alpha) \tag{24}$$

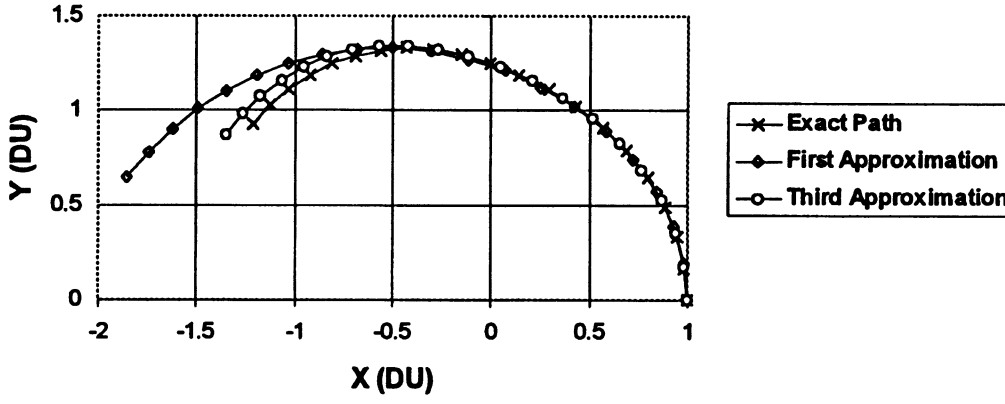

FIG. 12. Optimal Trajectory for Bryson and Ho Example.

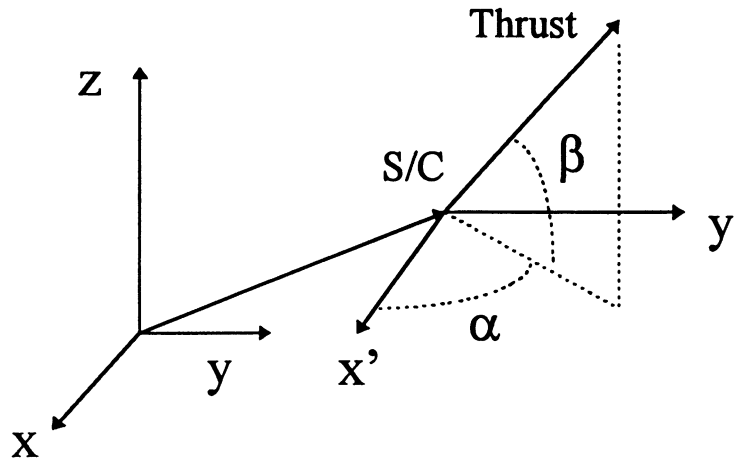

FIG. 13. Problem Geometry in Three Dimensions.

The costate equations are as follows:

$$\dot{\lambda}_x = \frac{\mu}{r^5}[\lambda_{\dot{x}}(y^2 + z^2 - 2x^2) - 3x(\lambda_{\dot{y}}y + \lambda_{\dot{z}}z)] \tag{25}$$

$$\dot{\lambda}_y = \frac{\mu}{r^5}[\lambda_{\dot{y}}(x^2 + z^2 - 2y^2) - 3y(\lambda_{\dot{x}}x + \lambda_{\dot{z}}z)] \tag{26}$$

$$\dot{\lambda}_z = \frac{\mu}{r^5}[\lambda_{\dot{z}}(x^2 + y^2 - 2z^2) - 3z(\lambda_{\dot{x}}x + \lambda_{\dot{y}}y)] \tag{27}$$

$$\dot{\lambda}_{\dot{x}} = -\lambda_x \tag{28}$$

$$\dot{\lambda}_{\dot{y}} = -\lambda_y \tag{29}$$

$$\dot{\lambda}_{\dot{z}} = -\lambda_z \tag{30}$$

It is possible to apply the two-dimensional initial costate approximations to a three-dimensional problem. The Lagrange costates associated with the z position and velocity, $\lambda_z(0)$ and $\lambda_{\dot{z}}(0)$ are unknown at the initial time. However, they may be set equal to zero as a reasonable starting guess for problems with inclination changes as high as 45 degrees, in some cases. This is because λ_z and $\lambda_{\dot{z}}$ are both always equal to zero if the transfer is confined to the x-y plane. Also, it has been shown previously [5] that the initial values $\lambda_y(0)$ and $\lambda_{\dot{x}}(0)$ are equal if the starting orbit is circular. Taking $\lambda_x(0) = 1$ in the same way that we set $\lambda_r(0) = 1$ previously, the set of states and costates are initialized as follows:

$$\begin{aligned}
x(0) &= 1, \quad \lambda_x(0) = 1 \\
y(0) &= 0, \quad \lambda_y(0) = \lambda_u(0) \\
z(0) &= 0, \quad \lambda_z(0) = 0 \\
\dot{x}(0) &= 0, \quad \lambda_{\dot{x}}(0) = \lambda_u(0) \\
\dot{y}(0) &= 1, \quad \lambda_{\dot{y}}(0) = \lambda_v(0) \\
\dot{z}(0) &= 0, \quad \lambda_{\dot{z}}(0) = 0
\end{aligned}$$

In the two-dimensional problem, the three final boundary conditions are R, the radial velocity, and the tangential velocity. This set of conditions could be used to define a circular orbit completely with a desired direction of rotation. In the three-dimensional problem, two more final conditions are necessary to correspond with the two new unknown initial costates, $\lambda_z(0)$ and $\lambda_{\dot{z}}(0)$. If the three components of the angular momentum vector are used along with the radial and tangential velocities, a total of five scalar boundary conditions are established. These quantities uniquely determine a circular orbit with a desired inclination and ascending node.

Three-Dimensional Examples

To show the relationships between the two- and three-dimensional cases, a two-dimensional example is first presented, then modified to include a 45 degree inclination change. All other parameters are held the same. Finally, an example is presented where the transfer is to an elliptical orbit with an inclination of 90 degrees. In all examples, the initial orbit is a unit circle in the x-y plane, and the starting point is at $x = 1$, $y = 0$. The final orbital states for each example are given in their individual descriptions and figures.

Coplanar Example

In Fig. 14, an optimal circle-to-circle transfer is shown where $R = 5$, $A = 0.1$, and $\dot{m} = -0.05$. In this case, the path covers more than a quarter revolution, but less than ten complete revolutions. Accordingly, the initial costates lie in the elliptic region of Fig. 4. To solve this problem, the parameterized elliptic curve fits are used to provide the approximate initial costate values.

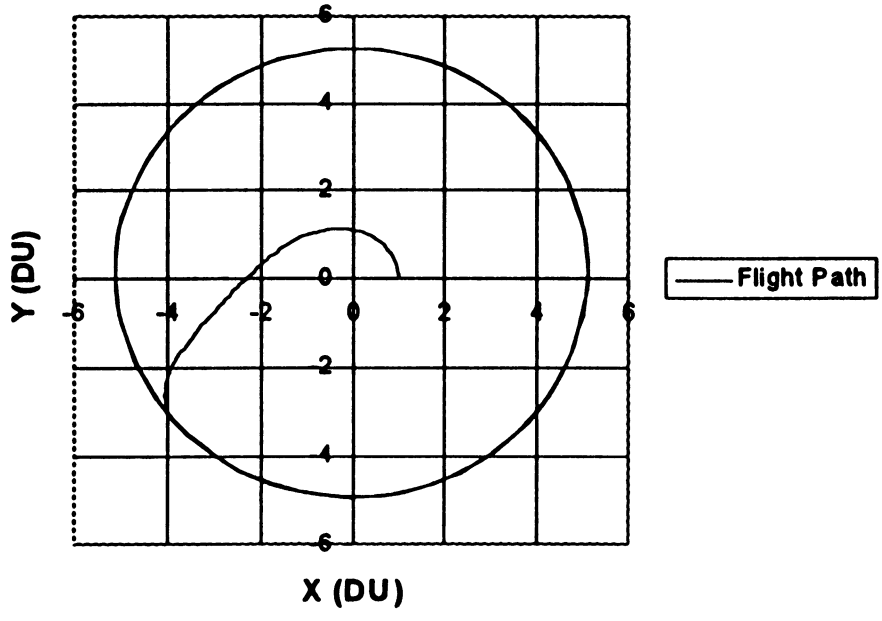

FIG. 14. Flight Path for Two-Dimensional Example.

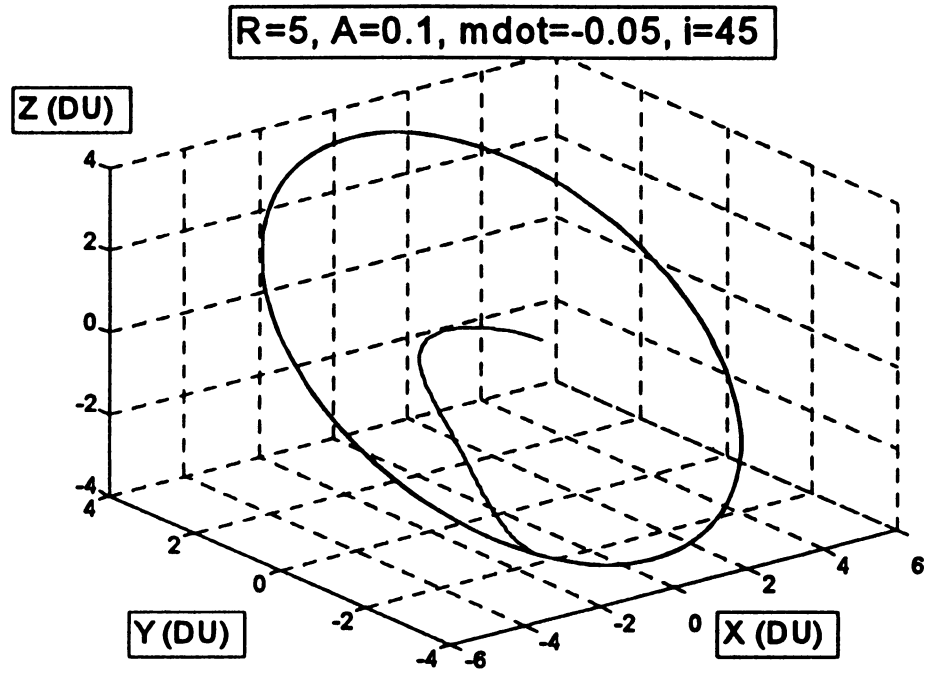

FIG. 15. Flight Path for Three-Dimensional Example.

Noncoplanar Example

In Fig. 15, the problem parameters are the same as in the example plotted in Fig. 14. However, the final circular orbit is inclined by 45 degrees. The right ascension of the ascending node is located at zero degrees, on the positive x-axis. The approximate initial values for λ_u and λ_v are the same as in the two dimensional case, and $\lambda_z(0)$ and $\lambda_{\dot{z}}(0)$ are taken to be zero. Convergence is achieved, even with a final inclination of 45 degrees.

In the two-dimensional case, the costates related to the z direction are zero throughout the transfer. Thus, the initial values should both be zero, as seen in Table 3. In the three-dimensional case, all of the costates vary with time. The right ascension of the ascending node is zero for this example, and choosing other angles will result in different values for the optimal initial costates and final time. Changes in A and R will affect the maximum inclination for which the initial values $\lambda_z(0) = 0$ and $\lambda_{\dot{z}}(0) = 0$ will lead to convergence.

Noncoplanar, Noncircular Example

As a final example, the optimal initial costates from the three-dimensional case in Table 3 are used as initial values to solve a problem with noncircular end conditions. In this case, the goal is to reach an elliptical, polar orbit at apoapse with $r(t_f) = 5$, where the tangential velocity is 0.4 DU/TU, which is much less than the circular velocity of 0.4472 DU/TU. The final orbit has an eccentricity of 0.2, a semi-major axis of 4.167 DU, and the right ascension of the ascending node is zero as before. The argument of periapsis is not specified, since we only seek the minimum time to a particular radius and velocity, not a specific point in space. Convergence is achieved using the values from Table 3 with no further

TABLE 3. Planar vs Noncoplanar Example

	Model	2D	3D, $i = 45$	3D, $i = 90$
$\lambda_x(0)$	1	1	1	1
$\lambda_y(0)$	−0.1092950	−0.239259	−0.190287	−0.161830
$\lambda_z(0)$	0	0	0.565053	0.353082
$\lambda_{\dot{x}}(0)$	−0.1092950	−0.239259	−0.190287	−0.161830
$\lambda_{\dot{y}}(0)$	1.1923589	1.278794	1.281757	1.550567
$\lambda_{\dot{z}}(0)$	0	0	0.443959	0.827519
t_f	12.6491106	10.045897	10.985076	14.437969
Iterations	1	12	14	18

modification. Taking large steps in this way by using previous results can allow for the solution of a wide variety of orbit transfer problems in a short time. In this case, the steps involve inclination changes of 45 degrees each time. The converged trajectory is shown in Fig. 16.

Both the first and second cases are solved using the two-dimensional approximations as initial values. The third case uses the results of the second case as initial values. The largest difference between the second and third cases is in the flight time. Some of the initial costates in the third case are actually closer to the approximate two-dimensional models than those in the second case. However, the difference in final time is apparently large enough to prevent convergence from the approximate models directly. For comparison, the final, converged values are shown in Table 3 for each case.

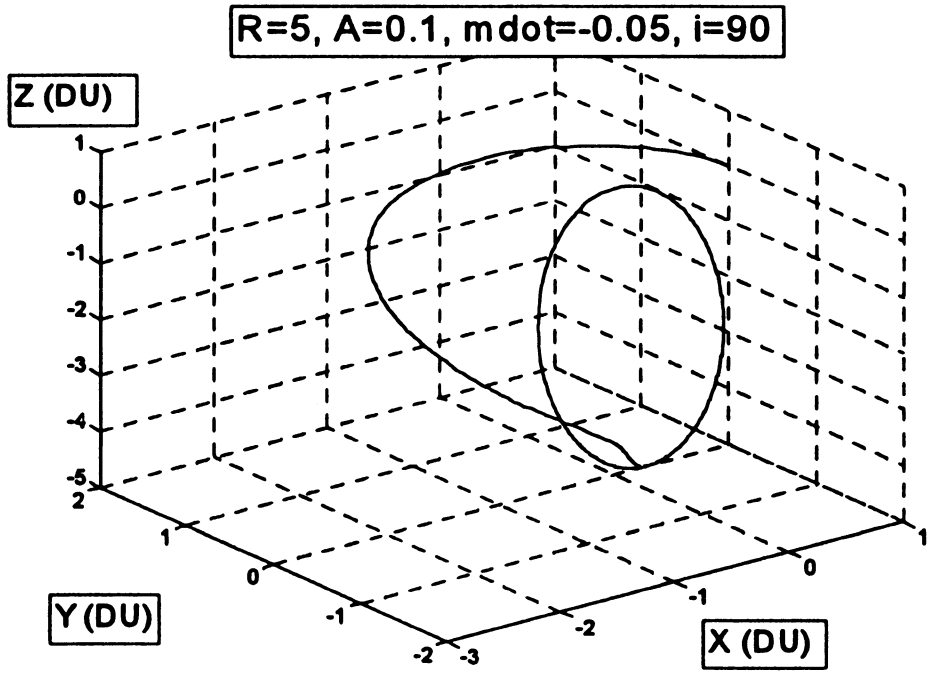

FIG. 16. Flight Path for Polar, Elliptical Example.

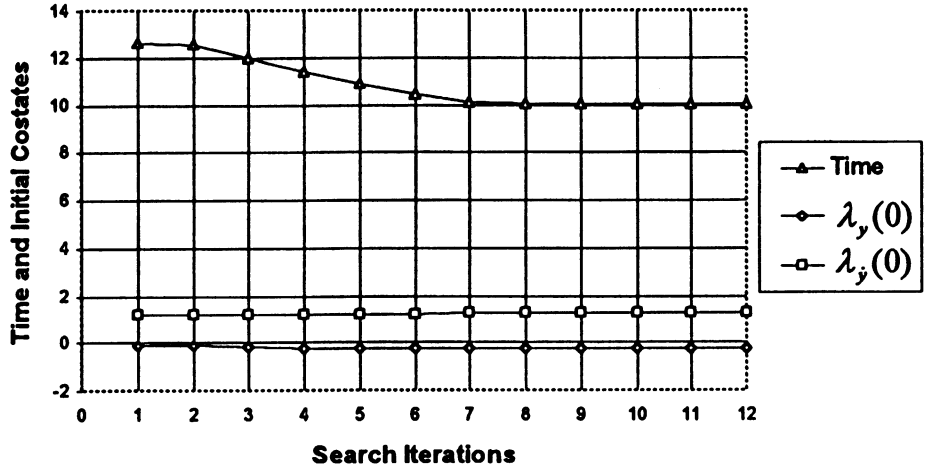

FIG. 17. Iterative Search History for Two-Dimensional Example.

Figures 17–19 show the iterative search histories for the flight time and initial costates in the two-dimensional, three-dimensional, and polar-elliptical examples from the initial approximations to the converged values. In these cases, convergence took 12, 14, and 18 iterations of the shooting method, respectively.

Figure 20 shows that the behavior of the thrust angle α is similar between the two-dimensional and three-dimensional cases, although the three-dimensional case has smoother "corners," which may be because it is not constrained to two dimensions. The thrust angle β starts off with similar behavior between the three-dimensional $i = 45$ deg case and the polar-elliptical example, and arrives at nearly the same final values for both cases. Figure 21 shows the control angle histories for α and β in the polar-elliptical example. The flattening of both curves at the end of the trajectory indicates the braking maneuver needed to arrive at apoapse.

In the two-dimensional case, the costates related to the z direction are zero throughout the transfer. In the three-dimensional case, all of the costates vary with time. The ascending node is zero for this example, and choosing other

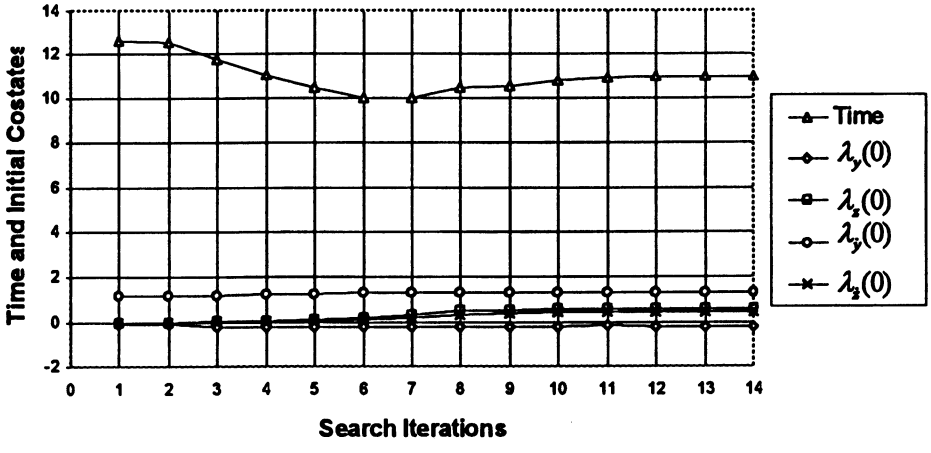

FIG. 18. Iterative Search History for Three-Dimensional Example ($i = 45$ deg).

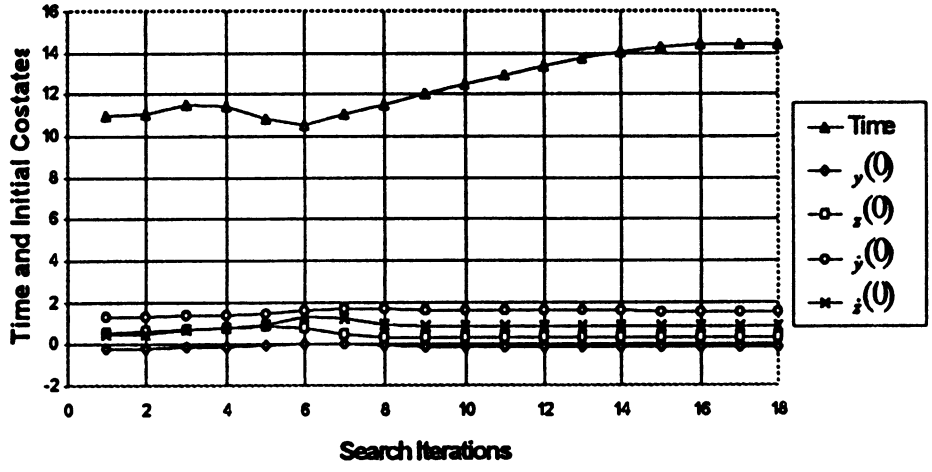

FIG. 19. Iterative Search History for Polar-Elliptical Example.

angles will result in different values for the optimal initial costates and final time. The best agreement between the two cases is for $\lambda_y(0)$ and $\lambda_{\dot{y}}(0)$, which may be approximated with equations (10) and (11). Convergence is achieved in 12 iterations of the shooting method for the first case, 14 iterations for the second case, and 18 iterations in the third case.

Conclusions

The initial costates for the planar minimum-time, circle-to-circle, continuous-thrust orbit transfer exhibit a consistent structure when the problem is posed in canonical units. This structure can be exploited to develop a globally effective approach to solving the associated two-point boundary value problems. Specifically, the locus of initial costates can be divided into three regions depending on a parameter involving the final orbit radius and the initial acceleration. The approximate initial costates developed for these three regions lead to reasonably

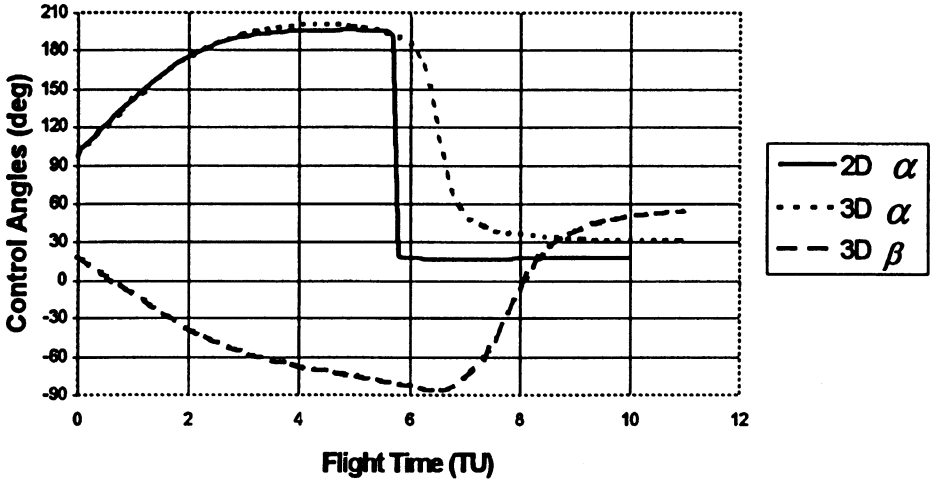

FIG. 20. Control Angle Histories for 2D and 3D (i = 45 deg) Examples.

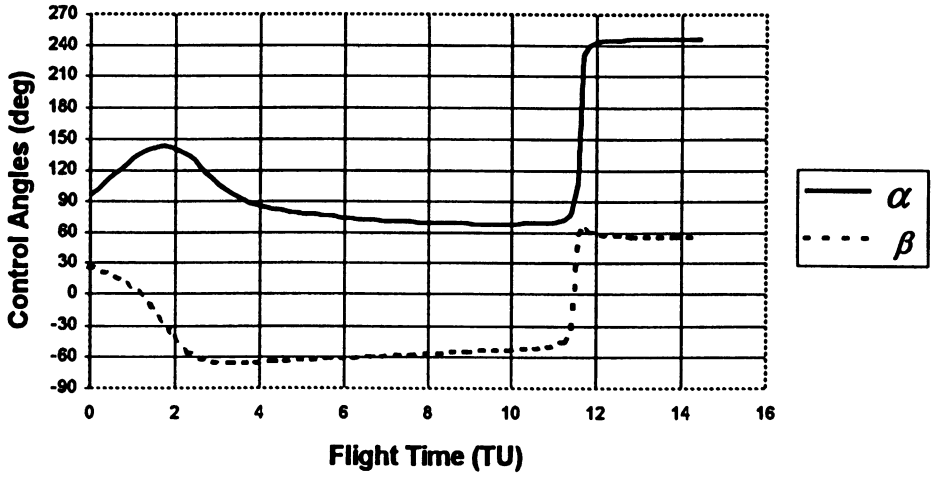

FIG. 21. Control Angle Histories for Polar-Elliptical Example.

quick convergence of a simple shooting method for any problem of interest, and do not require the usual continuation from a known solution. Furthermore, these approximations make it possible to obtain solutions to the more complicated three-dimensional orbit transfers and transfers where the final orbit is not circular.

References

[1] EDELBAUM, T. N. "Optimal Low-Thrust Rendezvous and Station Keeping," *AIAA Journal*, Vol. 2, No. 7, 1964, pp. 1196–1201.

[2] WIESEL, W. E., and ALFANO, S. "Optimal Many-Revolution Orbit Transfer," *Journal of Guidance, Control and Dynamics*, Vol. 8, No. 1, 1985, pp. 155–157.

[3] PRUSSING, J. E. "Equation for Optimal Power-Limited Spacecraft Trajectories," *Journal of Guidance, Control and Dynamics*, Vol. 16, No. 2, 1993, pp. 391–393.

[4] ALFANO, S., and THORNE, J. D. "Constant-Thrust Orbit-Raising," *Journal of the Astronautical Sciences*, Vol. 42, No. 1, 1994, pp. 35–45.

[5] THORNE, J. D., and HALL, C. D. "Approximate Initial Costates for Continuous-Thrust Spacecraft," *Journal of Guidance, Control and Dynamics*, Vol. 19, No. 2, 1996, pp. 283–288.

[6] SEYWALD, H. "Trajectory Optimization Based on Differential Inclusion," *Journal of Guidance, Control and Dynamics*, Vol. 17, No. 3, 1994, pp. 480–487.

[7] HERMAN, A. L., and CONWAY, B. A. "Direct Optimization Using Collocation Based on High-Order Gauss-Lobatto Quadrature Rules," *Journal of Guidance, Control and Dynamics*, Vol. 19, No. 3, 1996, pp. 592–599.

[8] RAUWOLF, G., and COVERSTONE-CARROLL, V. "Near-Optimal Low-Thrust Orbit Transfer Generated by Genetic Algorithms," *Journal of Spacecraft and Rockets*, Vol. 33, No. 6, 1996, pp. 859–862.

[9] BATE, R., MUELLER, D., and WHITE, J. *Fundamentals of Astrodynamics*, Dover Publications Inc., New York, 1971, pp. 40–43.

[10] BRYSON, A. E., and HO, Y. C. *Applied Optimal Control*, Hemisphere Publishing Co., Washington, D.C., 1975, pp. 66–69.

[11] PINES, S. "Constants of the Motion for Optimal Thrust Trajectories in a Central Force Field," *AIAA Journal*, Vol. 2, No. 11, 1964, pp. 2010–2014.

[12] REDDING, D. C., and BREAKWELL, J. V. "Optimal Low-Thrust Transfers to Synchronous Orbit," *Journal of Guidance, Control and Dynamics*, Vol. 7, No. 2, 1984, pp. 148–155.

[13] KIRK, D. E. *Optimal Control Theory–An Introduction*, Prentice-Hall Inc., Englewood Cliffs, New Jersey, 1970, Chapter 5.

[14] THORNE, J. D., and HALL, C. D. "Optimal Continuous-Thrust Orbit Transfers," Paper No. 96-197, AAS/AIAA Space Flight Mechanics Meeting, Austin, Texas, February 1996.

[15] THORNE, J.D. "Optimal Continuous-Thrust Orbit Transfers," Ph.D. Dissertation, AFIT/DS/ENY/96-7, Graduate School of Engineering, Air Force Institute of Technology, Wright-Patterson AFB, Ohio, June 1996.

[16] PRESS, W.H., FLANNERY, B.P., TEUKOLSKY, S.A., and VETTERING, W.T. *Numerical Recipes in C-The Art of Scientific Computing*, Cambridge University Press, Cambridge, 1988, Chapter 16.